

## Icosahedral packing of polymer-tethered nanospheres and stabilization of the gyroid phase

Christopher R. Iacovella,<sup>1</sup> Aaron S. Keys,<sup>1</sup> Mark A. Horsch,<sup>1</sup> and Sharon C. Glotzer<sup>1,2</sup>

<sup>1</sup>Department of Chemical Engineering, University of Michigan, Ann Arbor, Michigan 48109-2136, USA

<sup>2</sup>Department of Materials Science and Engineering, University of Michigan, Ann Arbor, Michigan 48109-2136, USA

(Received 17 May 2006; revised manuscript received 29 January 2007; published 16 April 2007)

We present results of simulations that predict the phases formed by the self-assembly of model nanospheres functionalized with a single polymer “tether,” including double gyroid, perforated lamella, and crystalline bilayer phases. We show that microphase separation of the immiscible tethers and nanospheres causes confinement of the nanoparticles, which promotes local icosahedral packing that in turn stabilizes the gyroid. We present a new metric for determining the local arrangement of particles based on spherical harmonic “fingerprints,” which we use to quantify the extent of icosahedral ordering.

DOI: [10.1103/PhysRevE.75.040801](https://doi.org/10.1103/PhysRevE.75.040801)

PACS number(s): 82.35.Np, 83.80.Uv, 81.16.Dn, 07.05.Tp

The ability of block copolymers (BCPs) to order into periodic microdomains makes them a choice building block for applications ranging from drug delivery [1] to photonic-band-gap materials [2]. The BCP bicontinuous phases, when modified with nanoparticles (NPs), are seen as ideal candidates for catalytic materials and high conductivity nanocomposites [3]. Polymer-tethered NPs provide a route for the self-assembly of ordered arrays of NPs where the bulk phases formed resemble the complex morphologies found in BCPs and surfactants [4–6]. Polymer-tethered NPs constitute a class of shape amphiphiles where microphase separation occurs due to the immiscibility between the NP and tether [6]. In these systems, the geometry of the NP influences the bulk structure and local arrangement of NP by inducing liquid crystalline ordering [4,6]. Simulations of polymer-tethered nanorods highlight the interplay between microphase separation and particle geometry; e.g., the phase behavior for tethered rods includes a chiral cylinder phase and ordered smectic phases [4], not observed in flexible BCPs. Additional work suggests that morphologies may adopt unique structures as a result of confinement, including helical structures formed by colloids confined in v-shaped grooves [7] and helices and tori formed from BCPs confined in cylindrical pores [8].

Here, we examine the bulk-phase microstructures formed by polymer-tethered nanospheres (TNS) with attractive particles and repulsive tethers and demonstrate via simulation the first NP-based double gyroid phase. We present a new metric of local order based on spherical harmonics and use this to explore the impact of microphase-separation-induced confinement on the local ordering of spherical particles. We show that this confinement promotes icosahedral packing of hard attractive particles, which helps to stabilize certain microphase-separated structures with limited stability in BCP systems, including the double gyroid.

To realize long time scales and large systems required to self-assemble complex mesophases, we use the method of Brownian dynamics (BD). We consider a general class of tethered NPs rather than any one specific system and use empirical pair potentials that have been successful in the study of BCPs and surfactants. Nanospheres are modeled as beads of diameter  $2.0\sigma$  connected to tethers via finitely extensible nonlinear elastic (FENE) springs. Tethers are modeled as bead-spring chains containing eight beads of diam-

eter  $\sigma$  connected via FENE springs. To model the attractive interaction between NPs we use the Lennard-Jones potential (LJ), where particle-particle distances are calculated between particle surfaces. Solvophilic tethers and species of different types interact via a purely repulsive Weeks-Chandler-Andersen (WCA) soft-sphere potential to account for short-range, excluded volume interactions. The natural units of these systems are  $\sigma$ , the diameter of a tether bead,  $m$ , the mass of a tether bead, and  $\epsilon$ , the LJ well depth. Volume fraction  $\phi$  is defined as the ratio of excluded volume of the beads to the system volume, the dimensionless time is  $t^* = \sigma\sqrt{m/\epsilon}$ , and the degree of immiscibility and solvent quality are determined by the reciprocal temperature,  $1/T^* = \epsilon/k_B T$ . Further details of the model and method can be found in [5,6]. This model relates well to experimentally synthesized building blocks including polymer-functionalized fullerenes [9], tethered NPs formed by crosslinking one block of a BCP [10], and tethered quantum dots [11].

**Bulk ordering.** To examine the bulk phase ordering of the TNS system with attractive NP headgroups, we explore the  $T^*$  vs  $\phi$  phase diagram. Simulations are conducted at ten fixed volume fractions between 0.15 and 0.45. Disordered systems are incrementally cooled until bulk ordered phases are reached, as determined by visual inspection and discontinuities in potential energy as a function of  $T^*$  [12]. For each  $\phi$ , multiple runs are conducted at various cooling rates and system sizes to avoid dynamically trapped structures and finite size effects. Our results presented are based on  $\sim 40$  independent runs of  $\sim 250$  state points for  $T^*$  between 0.21 and 2.0, for systems of 500–4000 TNS, (4500–36 000 individual beads). A phase diagram summarizing the observed phases is presented in Fig. 1; each data point represents a state point arrived at using multiple cooling rates and system sizes. With increasing  $\phi$ , we observe disordered wormy micelles (DWM), hexagonally packed cylindrical micelles (H), the bicontinuous double gyroid (DG), perforated lamellae with perforations through the NP layer (PLH), and lamellar bilayers (L). At  $T^* > T_{ODT}^*$ , we find disordered aggregates and at sufficiently high  $T^*$  we find no aggregates.

Interestingly, we observe both DG and PLH phases between  $\phi \sim 0.30$ – $0.45$ . A snapshot of the DG phase is shown in Fig. 2(a) and a snapshot of the PLH phase is shown in Fig. 2(b). In BCP systems, both the DG and PLH phases have

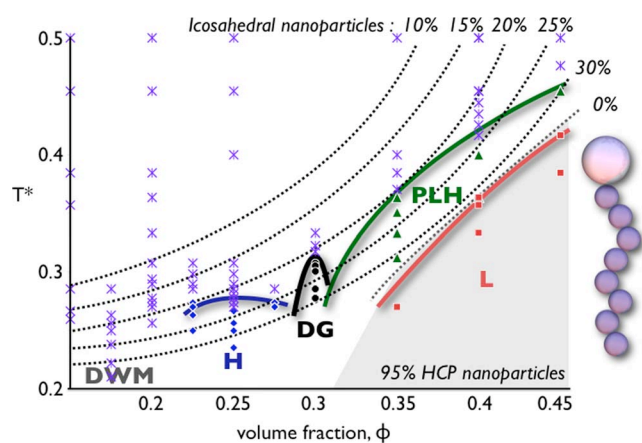


FIG. 1. (Color online)  $T^*$  vs  $\phi$  phase behavior, where solid lines represent approximate phase boundaries determined by  $\sim 250$  state points. Stars indicate simulated disordered phases. With increasing  $\phi$  we observe disordered wormy micelles (DWM), hexagonally packed cylinders (H), double gyroid (DG), perforated lamellae with perforations through the NPs (PLH), and lamellar bilayers (L). Dotted lines fit data points indicating values of  $T^*$  and  $\phi$  at which the indicated percentages of icosahedral clusters formed by NP head groups are found. The shaded region indicates the range of  $T^*$  and  $\phi$  over which crystalline ordering of the NPs is observed. A schematic of the model tethered nanosphere is shown at right.

been reported in similar regions of the phase diagram [13]; however, the DG phase is considered to be an equilibrium morphology [14] and the PLH phase is considered to be metastable, stabilized by compositional fluctuations [15]. Few examples of the DG phase exist for the simulation of

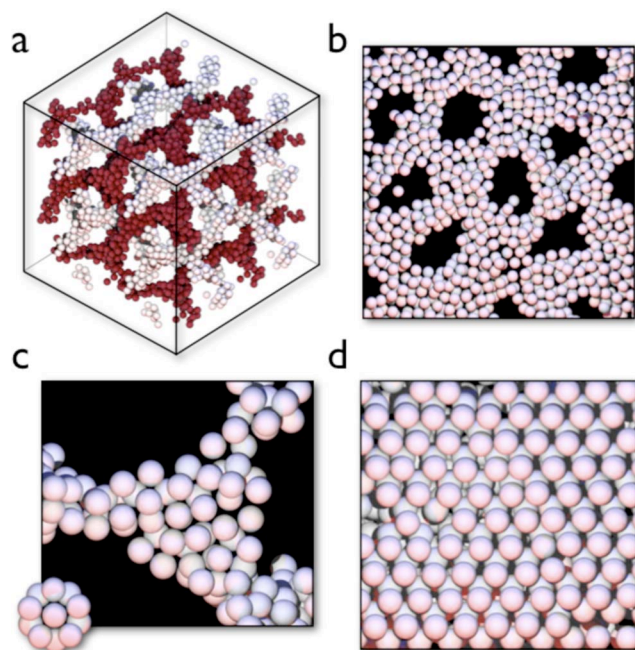


FIG. 2. (Color online) Images of self-assembled structures with tethers removed for clarity. (a) DG phase; the minimal unit cell was duplicated and found to be stable over  $\sim 10$  million time steps. (b) Individual sheet of PLH. (c) Node of the DG, showing icosahedral rings; perfect icosahedron inset. (d) Crystalline packing of L.

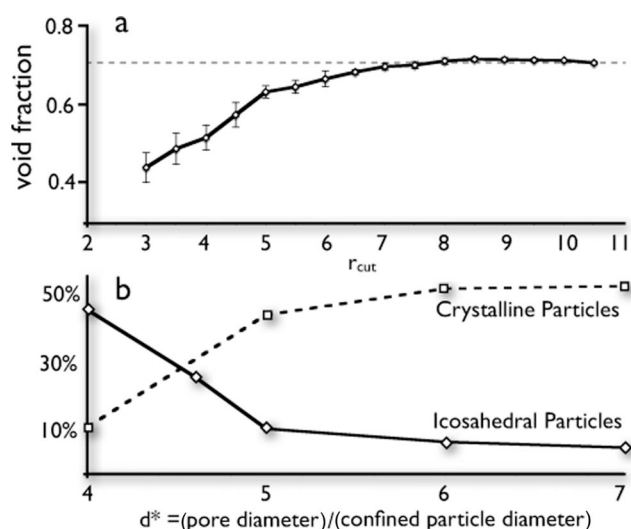


FIG. 3. (a) Void fraction of a node vs  $r_{cut}$ . For small  $r_{cut}$  values, void fraction is lower than the bulk, approaching the bulk value of 0.7 (dotted in figure) as  $r_{cut}$  is increased. (b) Percentage of icosahedral and crystalline NPs under cylindrical confinement vs  $d^*$ . Icosahedral ordering is favored for diameters less than 5, which corresponds to the diameter of the tubes formed in the DG and H phases.

BCPs and surfactants using off-lattice, dynamics-based methods [16,17]. For the TNS system, the dominance of the PLH phase outside of the DG region suggests that over this  $\phi$  range it is stable and reproducible; we did not observe bicontinuous structures within the PLH region. As in the case of the polymer-tethered rods, the perforations result from competition between the NPs tending to locally order and the tether tending to maximize its configurational entropy [4].

*Stability of the gyroid.* The limited stability of the DG phase in BCP systems has been attributed to packing frustration within the connection points (nodes) [18,19], which arises due to a high void fraction (low packing density) within the nodes. To examine this, we look at relative trends in void fraction. We approximate the center of a node and calculate the void fraction within a spherical volume drawn from the center, repeating for various sphere radii,  $r_{cut}$ . We find that for small values of  $r_{cut}$  the void fraction is lower than in the bulk, starting at  $\sim 0.44$ , and as  $r_{cut}$  is increased we approach the bulk void fraction of 0.7 as shown in Fig. 3(a). Thus particles within the nodes pack more densely than in the bulk. Reference [20] used a similar analysis to compare a monodisperse BCP system to a blend of two different length BCPs. In the blend, the authors found that the longer of the two polymers occupied the nodes of the DG, resulting in a larger range of stability compared to the monodisperse system [20]. For the monodisperse system, the authors found that the void fraction is higher than the bulk for small values of  $r_{cut}$ , and decays to the bulk value as  $r_{cut}$  becomes large [20]. In the blend, the authors found that, like our system, the void fraction is lower than the bulk for small values of  $r_{cut}$  and approaches the bulk value from below as  $r_{cut}$  becomes large [20]. This similarity in trends suggests that the ability of the TNS system to realize the DG phase is linked to the ability of NPs to locally order into dense structures, decreas-

ing the packing frustration. Figure 2(c) shows that NPs form ringlike structures resembling icosahedral clusters at the nodes. Unlike icosahedral ordering observed in dense liquids, the tether sterically restricts particle packing, resulting in clusters with only partial coordination.

*Characterizing local structures.* To characterize rigorously the local particle packing, we introduce a residual minimization scheme as a modification of the cluster shape-matching algorithm of Steinhardt *et al.* [21]. For a thorough explanation of the scheme of Steinhardt *et al.*, see [21–23]. Our scheme is general and can be applied to any liquid or crystalline system of spherical particles obtained via experiment or simulation.

We aim to determine if a set of vectors  $r$  drawn from a particle to its nearest neighbors matches a given reference structure (e.g., an icosahedron or an FCC crystal cluster). Because nonperiodic systems contain configurations with many different orientations, this analysis cannot be accomplished trivially by, e.g., applying a set of Cartesian vector dot products. The spherical harmonics construction of Steinhardt *et al.* allows for matching structures in a way that is independent of orientation.

To quantify the shape of a cluster two metrics of local ordering are defined:  $Q_l$  and  $w_l$ .  $Q_l$  is derived by evaluating a set of spherical harmonic functions  $Y_{lm}(\theta, \phi)$  for each nearest-neighbor direction  $\theta_i(r_i)$ ,  $\phi_i(r_i)$ , where  $l$  is the harmonic frequency and  $m$  is an integer that runs from  $-l$  to  $l$ . Summing over all bonds in the sample gives the  $2l+1$ -dimensional vector  $Q_l$ , which contains one component for each  $m$ . Because of the symmetries of spherical harmonics, the magnitude of the  $Q_l$  vector is invariant for a given cluster regardless of its orientation. The quantity  $w_l$  is derived by considering specific rotationally invariant combinations of the average values of the  $Q_l$  vector components  $Q_{lm}$ .

The typical implementation of the Steinhardt *et al.* scheme involves choosing one or two harmonics (usually  $l=4$  and  $l=6$ ) and comparing the resulting  $Q_l$  and  $w_l$  values for the local structure to the expected values of reference structures. In order to make this comparison it is necessary to define cutoff values that define a match (e.g., if  $Q_6 > 0.6$  and  $w_6 < -0.1$ , then the structure is locally an icosahedron [21]). This scheme works well for differentiating between two local structures [23], however, when attempting to differentiate between many structures this method becomes cumbersome, since cutoffs must be determined via trial and error. An additional subtle problem is that certain structures have similar values for particular harmonics (e.g., BCC and simple cubic have the same  $w_6$  value [24]). Thus, a given configuration may be misidentified when using such loosely defined cutoffs.

To avoid these problems, we introduce a residual-based scheme,  $R_{YLM}$ , that does not rely on multiple cutoffs or substantial trial and error. The first step in our scheme is to define a set of reference structures with which we wish to compare and determine their  $Q_l$  and  $w_l$  values for  $l=4, 6, \dots, 12$ . We only consider even number harmonics because they are invariant under inversion and because these frequencies are the leading terms in the expansion [21]. To determine the local configuration of a particle we calculate the residual value,  $\chi_i = \sqrt{\sum_{l=4}^{12} (Q_l - Q_{ref,l})^2 + \sum_{l=4}^{12} (w_l - w_{ref,l})^2}$ , with

respect to each reference structure. A particle is considered to be in the local configuration  $i$  that minimizes the residual  $\chi_i$ . By construction it is impossible to generate a reference structure for disordered local configurations, thus we classify a particle as belonging to a disordered local configuration if its residual exceeds a cutoff value, here chosen as 0.316. Only a single cutoff is required irrespective of the number of reference structures.

For the monatomic 12-6 LJ system, the  $R_{YLM}$  method is able to identify particles in a crystalline configuration with accuracy comparable to the local order parameter,  $q_6 \times q_6$  [24], which is a standard tool for analyzing crystals, but the  $R_{YLM}$  method allows us to classify structures by more than just “crystal-like” or “liquidlike” qualifiers.

*Quantifying local ordering.* To verify our visual findings, we incorporated into the  $R_{YLM}$  reference database icosahedral clusters that maintain the same bond angles, but possess only partial coordination numbers (e.g., we remove 1–4 particle(s) from a perfect 13-particle icosahedral cluster). These clusters are indistinguishable from the minimum potential energy clusters found by Doye and Wales [25]. Our reference library additionally contains other polyhedra and crystalline arrangements with full and partial coordination.

Applying the  $R_{YLM}$  algorithm to the DG phase, we confirm that the local arrangements of NPs are icosahedral with partial coordination as observed in Fig. 2(c). Applying this analysis to the entire  $T^*$  vs  $\phi$  phase diagram, we observe that as  $T^*$  is decreased, there is an increase in the number of icosahedrally ordered NPs with partial coordination corresponding to increased aggregation of NPs. Figure 1 shows the general trend of icosahedral ordering overlaid on the bulk phases; dotted lines indicate the set of values of  $T^*$  and  $\phi$  at which 10, 15, 20, 25, and 30% of the NPs are central particles in icosahedral clusters. Each line is interpolated from the analysis of the available data points (points at 6–16 different  $T^*$  for each  $\phi$ ), where each point is averaged over  $\sim 10$  samples or  $\sim 10\,000$  NPs. While we see a strong increase in icosahedral ordering, we see little increase in crystalline ordering until we reach the  $T_{ODT}^*$  of the  $L$  phase, at which point NPs crystallize and the number of icosahedrally-ordered NPs drops to nearly 0% (the shaded area in Fig. 1). There we find bilayers that possess distinct hexagonal closed-packed ordering of NPs as shown in Fig. 2(d), as compared to the liquidlike layers found in the PLH phase shown in Fig. 2(b).

*The role of confinement.* It is known that small clusters of LJ particles will favor icosahedral packing; however as the system size approaches bulk behavior, such ordering is lost in favor of close-packed crystals since icosahedra cannot tile Euclidean 3D space. The presence of icosahedral clusters in our systems is therefore surprising, since the domains contain many particles. The bulk phases that exhibit strong icosahedral ordering of NPs, namely, the H, DG, and PLH phases, have in common that the NP-rich domains are shaped like cylindrical tubes; the H and DG phases are clearly tubular and the PLH phase contains interconnected tubes arranged into sheets. We observe that there is little penetration of NPs into the polymer-rich domain, thus the boundary between these domains can be thought of as a confining surface. It appears that confining NPs into tubular domains, as a result of microphase separation, allows for the

formation of icosahedral clusters. To test this, we confine LJ particles of diameter  $2\sigma$  within cylindrical pores of various diameters with  $\phi=0.25$  and  $T^*=0.2$ . The interaction between the particles and the walls of the pore are modeled by the WCA potential. Examination of the dimensionless pore diameter,  $d^*=(\text{pore diameter})/(\text{confined particle size})$ , shows a strong presence of icosahedral particles with both full and partial coordination at  $d^* < 5$ , and an associated decrease in crystalline particles [Fig. 3(b)]. This model cylindrical pore system relates well to the tubular H and DG phases where  $d^* \sim 4.5-5$ .

Our results demonstrate the important role played by the local packing of NPs within microphase-separated domains

on the stability of the bulk structure for a tethered NP system. We observe a particularly interesting interplay between the local packing of NPs and domain shape, which stabilizes the DG phase and may be exploited in other tethered NP systems to stabilize even more complex structures. More generally, we find that cylindrical confinement, whether from hard walls or as a result of microphase separation, can be used to promote icosahedral ordering between attractive spheres.

We thank R. G. Larson, Z-L. Zhang, N. A. Kotov, the DOE (Grant No. DE-FG02-02ER46000) and DoEd (GAANN).

- 
- [1] K. Kataoka, A. Harada, and Y. Nagasaki, *Adv. Drug Delivery Rev.* **47**, 113 (2001).
- [2] M. Maldovan, A. M. Urbas, N. Yufa, W. C. Carter, and E. L. Thomas, *Phys. Rev. B* **65**, 165123 (2002).
- [3] B. K. Cho, A. Jain, S. M. Gruner, and U. Wiesner, *Science* **305**, 1598 (2004).
- [4] M. A. Horsch, Z. L. Zhang, and S. C. Glotzer, *Phys. Rev. Lett.* **95**, 056105 (2005).
- [5] C. R. Iacovella, M. A. Horsch, Z. Zhang, and S. C. Glotzer, *Langmuir* **21**, 9488 (2005).
- [6] Z. L. Zhang, M. A. Horsch, M. H. Lamm, and S. C. Glotzer, *Nano Lett.* **3**, 1341 (2003).
- [7] Y. D. Yin and Y. N. Xia, *J. Am. Chem. Soc.* **125**, 2048 (2003).
- [8] B. Yu, P. C. Sun, T. C. Chen, Q. H. Jin, D. T. Ding, B. H. Li, and A. C. Shi, *Phys. Rev. Lett.* **96**, 138306 (2006).
- [9] T. Song, S. Dai, K. C. Tam, S. Y. Lee, and S. H. Goh, *Langmuir* **19**, 4798 (2003).
- [10] Y. Kim, J. Pyun, J. M. J. Frechet, C. J. Hawker, and C. W. Frank, *Langmuir* **21**, 10444 (2005).
- [11] S. Westenhoff and N. A. Kotov, *J. Am. Chem. Soc.* **124**, 2448 (2002).
- [12] E. R. Chan, X. Zhang, C. Y. Lee, M. Neurock, and S. C. Glotzer, *Macromolecules* **38**, 14 (2005).
- [13] M. Imai, A. Kawaguchi, A. Saeki, K. Nakaya, T. Kato, K. Ito, and Y. Amemiya, *Phys. Rev. E* **62**, 6865 (2000).
- [14] D. A. Hajduk, P. E. Harper, S. M. Gruner, C. C. Honeker, G. Kim, E. L. Thomas, and L. J. Fetters, *Macromolecules* **27**, 4063 (1994).
- [15] I. W. Hamley, K. A. Koppi, J. H. Rosedale, F. S. Bates, K. Almdal, and K. Mortensen, *Macromolecules* **26**, 5959 (1993).
- [16] F. J. Martinez-Veracoechea and F. A. Escobedo, *J. Chem. Phys.* **125**, 104907 (2006).
- [17] I. Rychkov, *Macromol. Theory Simul.* **14**, 207 (2005).
- [18] M. W. Matsen and F. S. Bates, *Macromolecules* **29**, 7641 (1996).
- [19] H. Hasegawa, T. Hashimoto, and S. T. Hyde, *Polymer* **37**, 3825 (1996); E. W. Cochran, C. J. Garcia-Cervera, G. H. Fredrickson, *Macromolecules* **39**(7), 2449 (2006).
- [20] F. J. Martinez-Veracoechea and F. A. Escobedo, *Macromolecules* **38**, 8522 (2005).
- [21] P. J. Steinhardt, D. R. Nelson, and M. Ronchetti, *Phys. Rev. B* **28**, 784 (1983).
- [22] M. Kazhdan, T. Funkhouser, and S. Rusinkiewicz, *Rotation Invariant Spherical Harmonic Representation of 3D Shape Descriptors*, 882392 (2003), pp. 156–164.
- [23] P. R. tenWolde, M. J. Ruizmontero, and D. Frenkel, *Phys. Rev. Lett.* **75**, 2714 (1995).
- [24] P. R. tenWolde, M. J. Ruiz-Monterio, and D. Frenkel, *J. Chem. Phys.* **104**, 9932 (1996).
- [25] J. P. K. Doye, D. J. Wales, and S. I. Simdyankin, *Faraday Discuss.* **118**, 159 (2001).